Vet Clin Small Anim 37 (2007) 879–900
VETERINARY CLINICS
SMALL ANIMAL PRACTICE

# Advances in Respiratory Imaging

Eric G. Johnson, DVM*, Erik R. Wisner, DVM

Department of Surgical and Radiological Sciences, School of Veterinary Medicine, Veterinary Medical Teaching Hospital Small Animal Clinic, University of California at Davis, 1 Shields Avenue, Davis, CA 95616, USA

Imaging for the diagnosis of respiratory disease has routinely involved conventional radiography of the affected area. With the expanded availability of CT, this modality has demonstrated its usefulness in enhancing the sensitivity and specificity of respiratory imaging as a diagnostic tool. This article focuses on some of the newer approaches to imaging diagnoses and introduces the tomographic features of common respiratory disorders.

## SINONASAL DISORDERS

### Equipment and Technique

Radiographic studies of the nasal cavity and associated paranasal sinuses should include lateral and open- and closed-mouth ventrodorsal views to assess the nasal cavity fully, oblique projections to evaluate the osseous boundaries of the nasal cavity and paranasal sinuses, and a rostrocaudal projection to highlight the frontal sinuses. Animals must be under general anesthesia to achieve these views. At the authors' institution, all radiographic studies are acquired using a digital radiographic system (Eklin digital radiographic plate with Cannon image processing software, Eklin Medical Systems, Inc., Santa Clara, California) and resulting images are viewed on 3-megapixel gray-scale monitors. High-detail film screen combinations are also an excellent method for obtaining diagnostic nasal radiographs.

With the relatively recent advances in CT technology and design, the time required to complete studies has decreased dramatically. In fact, the time required to complete a CT scan of the nasal cavity is usually less than that required to perform conventional skull radiographs. At the authors' institution, a single-slice helical CT scanner (GE HiSpeed Advantage x/i; GE Medical Systems, Milwaukee, Wisconsin) is used. Patients are anesthetized and positioned in sternal recumbency, and 3- to 7-mm helical images (120 kV, 100 mA) of the skull are acquired from the tip of the nasal planum to the retropharyngeal lymph nodes. Images are viewed in stack mode on a workstation and evaluated

*Corresponding author. *E-mail address*: egjohnson@ucdavis.edu (E.G. Johnson).

0195-5616/07/$ – see front matter
doi:10.1016/j.cvsm.2007.05.004

in a wide bone window (window width = 2500, window level = 480) as well as in a narrow soft tissue window (window width = 340, widow level = 25). Thinner images (1–2-mm collimation) are often acquired to evaluate abnormalities detected on the initial images more fully. Intravenous contrast material can be useful in determining the extent and pattern of contrast enhancement of a nasal lesion. For neoplastic nasal masses, contrast media administration is also used to help further delineate tumor margins and to assess lymph nodes for evidence of regional metastasis.

## Inflammatory Nasal Disorders

### *Foreign body rhinitis*

Radiographic diagnosis of nasal foreign bodies depends on whether the object is radiopaque. Wood or grass foreign bodies are not directly identified, and radiographic findings are often minimal [1]. Radiopaque foreign bodies are not usually a diagnostic challenge; however, orthogonal radiographic projections are needed to confirm anatomic location accurately. Chronic nasal foreign bodies may result in radiographic evidence of unilateral increased soft tissue opacity or in focal destructive rhinitis [1].

CT seems to be more sensitive and specific than radiographic studies for diagnosis of nasal foreign bodies. CT characteristics of nasal foreign bodies may include direct visualization of the foreign body, evidence of localized turbinate destruction, or minimal to moderate localized soft tissue opacity surrounding the foreign body [2]. CT also provides a detailed map of the nasal passages to guide rhinoscopic nasal foreign body retrieval.

### *Fungal rhinitis*

The typical radiographic features of canine nasal aspergillosis have been defined as loss of turbinate architecture, especially rostrally, and thickening of the frontal bone [3]. Frontal sinus involvement is variable and is often identified as soft tissue density within the frontal sinuses.

The CT features of canine nasal aspergillosis have been described as destruction of the nasal turbinates with resulting cavitation of the affected nasal passage; focal or regional accumulation of abnormal soft tissue in the nasal passages; thickening of the mucosa of the frontal sinus, nasal cavity, and maxillary recess; and thickened reactive bone [4]. In many dogs, fungal granulomas of mixed gas and soft tissue opacity are present in the frontal sinus or caudal nasal cavity. In a few affected dogs, erosive bone destruction may also be evident, which can mimic the appearance of nasal neoplasia. Early in the course of disease, imaging findings are almost always unilateral with extension to the ipsilateral frontal sinus. Later in the disease process, the contralateral nasal cavity and frontal sinus may also be affected, although the disease remains unilateral in most dogs [4]. This constellation of CT features is highly characteristic of aspergillosis, and a diagnosis is highly suspected based on CT imaging findings alone. It has been shown that CT is far more sensitive than radiography for the detection and diagnosis of canine nasal aspergillosis lesions (Fig. 1) [5].

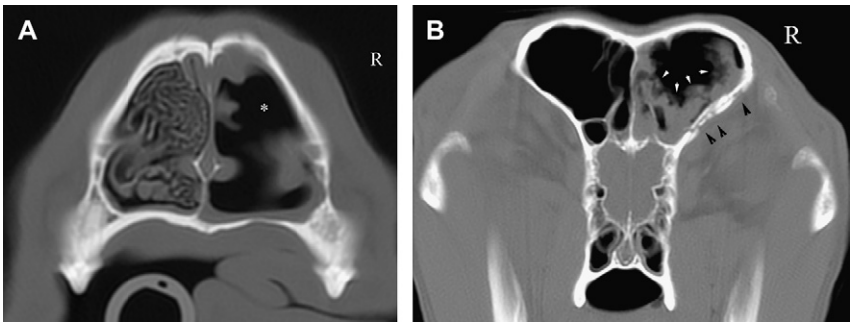


**Fig. 1.** (*A*) CT image at the level of the third maxillary premolar in a 4-year-old mixed-breed dog with a history of unilateral mucoid nasal discharge demonstrates cavitary destruction of the right nasal turbinates (*) with a region of abnormal soft tissue opacification affecting the right nasal passage. (*B*) CT image at the level of the frontal sinuses reveals thickened mucosa with mixed amorphous gas and soft tissue opacity within the right frontal sinus (*white arrows*). Additionally, there is a mixed productive and destructive bony change associated with the ventral floor of the right frontal sinus (*black arrowheads*). These findings are highly suggestive of nasal aspergillosis, which was confirmed with rhinoscopy and histopathologic examination.

Feline fungal rhinitis is most often attributable to infection with *Cryptococcus* rather than *Aspergillus* species. *Cryptococcus neoformans* is saprophytic yeast and is the most common systemic mycotic infectious organism in cats. Typically, this organism produces a hyperplastic rather than destructive rhinitis [6]. If fungal granulomas form in later stages of the disease, however, these may expand to destroy nasal turbinates and paranasal bones. *Aspergillus* rhinitis is rare in cats and may appear as a destructive rhinitis with radiographic and CT features similar to those of canine aspergillosis. Imaging features include profound destruction of the turbinate bones, increased soft tissue density in the nasal cavity, and frontal and sphenoid sinus fluid accumulation [7].

### *Nonspecific rhinitis in the dog*

*Nonspecific rhinitis* is a general term encompassing inflammatory nasal conditions. Radiographs can be normal or range from a unilateral or bilateral increase in opacity within the nasal passages. The paranasal sinuses may or may not be involved [1].

The CT changes of nonspecific rhinitis are typically mild, although cases vary in severity and laterality. They may include a bilateral nondestructive process with minimal to marked mucosal thickening and nasal fluid accumulation. Occasionally, there may be minimal to moderate fluid accumulation in the frontal sinuses and mild or moderate turbinate destruction, typically without overt destruction of cortical bone forming nasal cavity and sinus boundaries [2].

### *Canine nasal neoplasia*

Many types of tumors can arise within the canine nasal cavity, largely because of the many different cell types in this area. The most common nasal tumors are carcinomas, with adenocarcinoma being the most common. Definitive

diagnosis of nasal neoplasia requires biopsy, but imaging features of nasal neoplasia may lead to a presumptive diagnosis with a high degree of confidence. Radiographic signs of nasal neoplasia include erosion of the facial bones and vomer bones in addition to destruction of the normal turbinate pattern with increased soft tissue opacity within the nasal passages [1,8]. Frontal sinus involvement, appearing as fluid opacity replacing the normal air-filled cavities, is often identified secondary to obstruction of the nasofrontal aperture or secondary to direct extension of the tumor into one or both frontal sinuses.

CT is far more sensitive than conventional radiography for the detection of abnormalities of the nasal passages and skull attributable to nasal neoplasia in dogs [9]. CT allows for a more complete evaluation of the nasal cavity, endoturbinates and ectoturbinates, retrobulbar space, cribriform plate, frontal sinuses, and associated structures by removing superimposition of adjacent structures. Common CT findings of nasal neoplasia include ethmoid bone destruction, destruction of the nasal bone or maxilla, abnormal soft tissue in the retrobulbar space, moderate to severe turbinate destruction, frontal sinus fluid with soft tissue accumulation, a mass-like lesion in the nasal cavity, and patchy areas of increased attenuation within a soft tissue density (Fig. 2) [2,10]. CT also provides excellent guidance for rhinoscopy and nasal biopsy collection. Occasionally, if a large enough defect is identified in the nasal or paranasal bones using CT, ultrasound guidance can be used to obtain core biopsies of intranasal or perinasal masses.

Contrast medium uptake may be extremely nonuniform and frequently does not delineate tumor margins accurately. Because the CT features described often lead to a presumptive diagnosis of nasal neoplasia, the authors administer

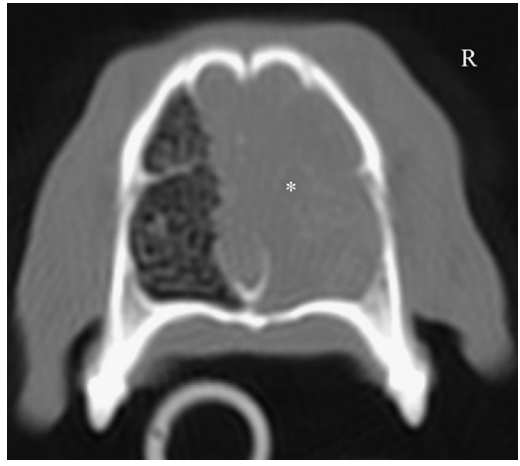


**Fig. 2.** CT image of the nasal cavity in a 10-year-old Sheltie presented with a 2-month history of right nasal epistaxis reveals a mass lesion in the right nasal cavity with destruction of the nasal septum and underlying nasal turbinates (*). Histopathologic examination confirmed nasal carcinoma.

intravenous iodinated contrast media to delineate tumor margins only when a breach of the paranasal bones has occurred. This helps to determine whether frontal sinus opacity is attributable to extension of nasal tumor or secondary to obstructive rhinitis. In the authors' experience, if complete opacification of one or both frontal sinuses is present, there is a high likelihood of nasal neoplasia. If the cribriform plate is disrupted, the degree of neoplastic extension into the calvarium can be more accurately assessed after administration of contrast. Contrast material administration can also help to evaluate the enhancement pattern of regional lymph nodes.

It is not possible to differentiate carcinoma from sarcoma based on radiographic or CT findings because they share many imaging characteristics. Definitive diagnosis of nasal neoplasia requires biopsy with histopathologic examination. Sarcomas of the nasal passages include chondrosarcomas, osteosarcomas, and multilobular osteochondrosarcomas as well as soft tissue sarcomas. Tumors that arise from the paranasal bones are more likely to be osteosarcomas or multilobular osteochondrosarcomas (Fig. 3). Chondrosarcomas typically appear aggressive and invasive, with regions of paranasal bone lysis. Spicules of mineralization can often be identified dissecting through these mass lesions.

Canine nasal lymphoma, although uncommon, has been documented multiple times at the authors' institution. Lymphoma can mimic the radiographic and CT findings of carcinomas and sarcomas, but its appearance is often less aggressive. CT features may include mild to moderate soft tissue opacification of the nasal passages, minimal turbinate destruction, and small multifocal nodules adjacent to turbinates. More aggressive appearing lesions are also possible,

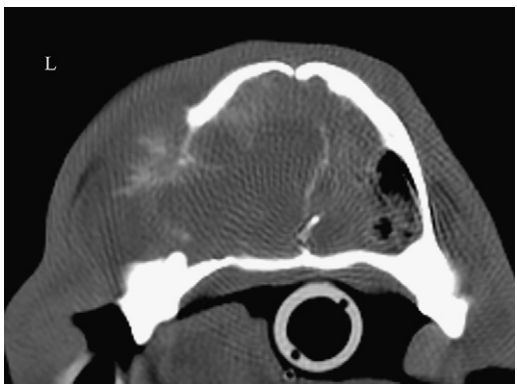


**Fig. 3.** CT image of a 7-year-old Pit Bull Terrier presented with unilateral epistaxis and swelling of the left side of the muzzle. This image illustrates a primarily destructive lesion centered around the left nasal and maxillary bone. There is a soft tissue mass effect in the left nasal cavity that extends through the nasal septum into the right nasal passage. Irregular new bone formation is identified around the left nasal bone within the associated soft tissue mass. Histopathologic examination was diagnostic for nasal osteosarcoma.

including large space-occupying nasal masses with associated bone loss. Nasopharyngeal soft tissue masses or polypoid lesions also are a common concurrent feature and may be the only significant CT finding. Adjacent lymph node enlargement is often not a concurrent feature (Fig. 4).

*Feline sinonasal disease*

Unlike the imaging findings in dogs, radiographic features of feline chronic rhinitis and sinonasal neoplasia are similar. Nasal carcinoma is a commonly reported neoplasm in the cat [11], although recent studies report lymphoma as a common tumor type as well [12,13]. Radiographic features reported with chronic rhinitis and nasal neoplasia include opacification of the frontal sinuses and nasal cavity; loss of definition of the nasal turbinates; a soft tissue mass effect; bony changes, including erosions of the paranasal bones, nasal septum, and nasal conchae; and deviation of the nasal septum. Radiographic changes more suggestive of feline nasal neoplasia than rhinitis include unilateral lysis of the paranasal bones, unilateral nasal turbinate destruction, and loss of teeth [13].

In feline nasal disease, CT is more sensitive than radiographs for detecting nasal cavity disorders and is more accurate for determining the anatomic extent of disease. CT abnormalities in nasal neoplasia are quite similar to the CT findings in chronic nasal disease, however, thus making nasal biopsy necessary for diagnosis. CT findings in both disease processes include deviation of the nasal septum, cribriform plate destruction, turbinate destruction, frontal sinus involvement, destruction of the paranasal bones, and involvement of extrasinonasal structures. Feline nasal neoplasia and inflammatory nasal diseases often


**Fig. 4.** CT image of a 3-year-old Rhodesian Ridgeback dog with a history of sneezing, stertor, and nasal discharge. There is soft tissue–attenuating material dissecting through the right ethmoturbinates and extending into the right frontal sinus. There is mild osteolysis of the vertical portion of the frontal bone (*black arrows*). A soft tissue polypoid mass can be seen within the nasopharyngeal meatus (*). Immunocytochemistry of fine needle aspirates was diagnostic for B-cell lymphoma.

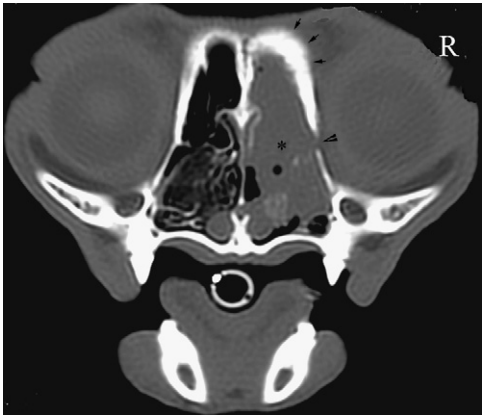


**Fig. 5.** CT image at the level of the orbits in an 8-year-old Scottish Fold presented with a history of chronic sneezing and nasal discharge shows soft tissue opacification of the right nasal passage with underlying turbinate loss (*). There is hyperostosis of the dorsal maxillary bone (*arrows*) with osteolysis of bone at the junction of the maxillary bone with the lacrimal bone (*arrowhead*). Rhinoscopy and biopsy demonstrated chronic neutrophilic and lymphoplasmacytic rhinitis.

involve both nasal cavities (Fig. 5) [12]. CT findings more suggestive of feline sinonasal neoplasia include bony change of the maxillary, lacrimal, and palatine bones; severe maxilloturbinate destruction; and pathologic changes of the facial soft tissues and orbit by extension. Also, identification of a homogeneous space-occupying mass with destruction of the nasal septum is highly suggestive of nasal neoplasia (Fig. 6) [12].

## THORAX

Conventional film radiology continues to be the mainstay of thoracic imaging. With the advent of helical CT technology, however, CT has become an important adjunct to the diagnostic evaluation of thoracic disorders. In general, CT provides better lesion characterization and delineation than conventional radiography for many thoracic disorders. Recognizing that thoracic radiography is the first diagnostic imaging step for patients with thoracic disease, the remainder of this section focuses on CT imaging features of commonly encountered thoracic disorders.

## THORACIC CT

### Equipment

Thoracic CT is best performed on third- or fourth-generation helical machines using a forced single-breath-hold helical scanning technique. Multiple detector arrays are now available that greatly reduce scan times; however, single detector arrays are adequate and often more economically feasible. At the authors' institution, images are obtained on a single-slice helical CT scanner (GE

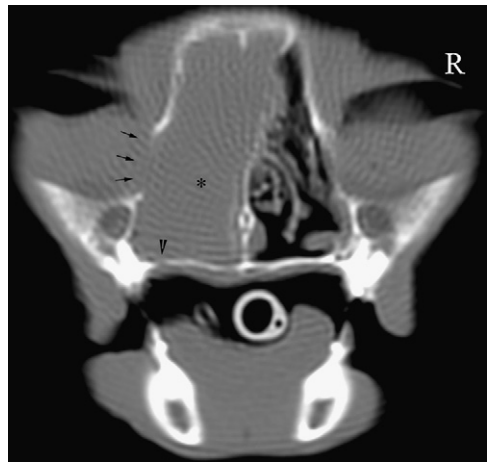


**Fig. 6.** CT image at the level of the rostral zygomatic arch in a 13-year-old domestic shorthaired cat presented with a history of nasal discharge and sneezing demonstrates a homogeneous space-occupying mass with destruction of the nasal septum (*). Destruction is identified at the junction of the maxillary, lacrimal, and frontal bones (*arrows*). Subtle destruction is also identified involving the palatine bone (*arrowhead*). Rhinoscopy with histopathologic examination was diagnostic for nasal lymphoma.

HiSpeed Advantage x/i). Animals are placed under general anesthesia and are maintained in dorsal or ventral recumbency to avoid atelectasis, which often occurs if the patients are transported to the CT gantry in lateral recumbency. The patients are manually hyperventilated just before the helical scan to decrease inspiratory drive during the forced breath hold. Contiguous helical images of the entire thorax are acquired using a slice collimation of 3 to 7 mm depending on the size of the patient. The slice thickness is chosen to allow the thorax to be scanned under a single breath hold that does not exceed 50 to 60 seconds. Images are evaluated in stack mode on a workstation in a lung window (window width = 2000, window level = 650) and a mediastinal window (window width = 750, window level = 70). When necessary, thinner slices are obtained through regions of pathologic findings recognized on the initial scan.

## Mediastinal and Pleural Space Disorders

### *Mediastinal masses*

Mediastinal masses can be localized to the cranial, middle, or caudal reflection of the mediastinum. Common mediastinal masses include thymoma, lymphoma, mediastinal cysts, and, occasionally, sarcomas. Often, radiographs in conjunction with ultrasonographic interrogation of the region are diagnostic for the presence of a mass or cyst. Conventional radiography and ultrasound are poorly sensitive for determining if a mediastinal lesion is aggressive with respect to vascular invasion; displacement of normal mediastinal structures

(eg, vasculature, esophagus); and invasion of adjacent structures, such as the thoracic wall or adjacent lung, however. For these reasons, CT is the method of choice for evaluating mediastinal masses in people [14]. In dogs and cats, CT of the mediastinum is useful for surgical planning, specifically for determining approximate tumor margins and the presence and extent of vascular invasion and to evaluate for nonradiographically apparent spread of disease, such as regional lymph node or pulmonary metastasis [15].

*Chylothorax*

Chylothorax is a condition characterized by accumulation of chyle within the pleural space that leads to respiratory impairment. Although chylothorax manifests as a pleural space disease, it results from pathologic change associated with the thoracic duct or its tributaries that reside within the mediastinum. In patients with chronic chylothorax, radiographs typically reveal variable amounts of pleural effusion, reduction in lung lobe volume, rounding of the lobar margins, and pleural thickening. In patients with idiopathic chylothorax, imaging of the thoracic duct is typically performed before surgical intervention. In veterinary medicine, this has traditionally been performed by surgical catheterization of an intestinal lymphatic vessel, followed by fluoroscopic and radiographic examination during lymphatic injection of iodinated contrast material. This technique is useful for defining the inherently variable anatomy of the thoracic duct and for demonstrating the location and character of the ductal lesion [16].

Recently, several studies have been performed to define the CT imaging characteristics of the canine thoracic duct. One study used traditional catheterization of a mesenteric lymphatic vessel and subsequent injection of iodinated contrast material to opacify the thoracic duct. This study was performed in normal dogs and suggested that CT can be used to define the number and location of thoracic duct branches more accurately than traditional radiographic lymphangiography [17]. Another study performed in dogs with presumed idiopathic chylothorax used a closed abdominal technique for opacification of the thoracic duct before thoracic CT. This technique involved direct lymphangiography by means of ultrasound-guided mesenteric lymph node injection of nonionic iodinated contrast material to achieve thoracic duct opacification. This technique provides excellent contrast enhancement of the thoracic duct and has documented dilated, tortuous, cranial mediastinal lymphatics that seem to be similar to idiopathic cranial mediastinal lymphangiectasia (Fig. 7) [18].

*Pyothorax*

Pyothorax is typically diagnosed in an animal with radiographic evidence of pleural effusion by performing pleural fluid analysis and culture. Radiographic features include unilateral or bilateral pleural fluid accumulation, reduction of aerated lung volume, and rounding or thickening of pleural margins. Occasionally, pleural adhesions involving the thoracic wall or diaphragm may occur [1]. Real or apparent alveolar pulmonary infiltrates may occur in patients with concurrent foreign body migration, pulmonary abscessation, or atelectasis. Pleural


**Fig. 7.** CT image of a 4-year-old Rottweiler at the level of the second sternebral segment after mesenteric lymph node injection with iodinated contrast material. There is excellent opacification of dilated cranial mediastinal lymphatic vessels consistent with idiopathic cranial mediastinal lymphangiectasia. Contrast material is present in the pleural space surrounding the left cranial lung lobe consistent with leakage from a mediastinal lymph vessel or vessels (*arrows*).

fluid often obscures thoracic structures, and repeat radiographic examination after removal of the fluid can be useful in evaluating the pulmonary parenchyma and cardiac silhouette.

CT may be indicated in patients with pyothorax that do not respond to conventional management techniques and in patients in which a pleural or pulmonary foreign body or abscess is suspected. Because of the cross-sectional nature of CT, superimposition and silhouetting of structures caused by loculated or residual pleural fluid are eliminated. CT findings associated with pyothorax include pleural and mediastinal fluid accumulation, encapsulated fluid accumulation (pleural abscess), thickening and rounding of pleural margins, thickening of mediastinal pleura, mild to moderate mediastinal and hilar lymphadenopathy (more significant with fungal organisms), pulmonary atelectasis, pulmonary alveolar infiltrates, and, occasionally, pleural adhesions.

CT can also reveal a pulmonary abscess, which typically appears as a thick-walled fluid-filled structure that may contain a gas-fluid interface. It can be difficult to differentiate an infected neoplasm from a primary pulmonary abscess. Chronic foreign bodies may lead to pulmonary abscessation, (Fig. 8) or may appear as focal regions of alveolar infiltrates surrounded by bronchiectatic airways.

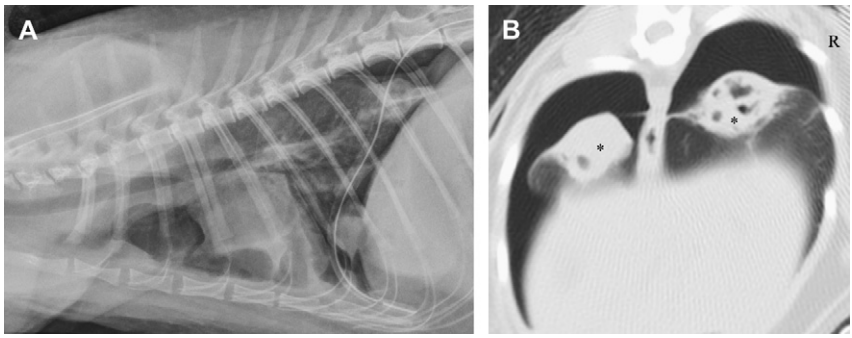


**Fig. 8.** Images from a 2-year-old cat with a history of pyothorax that was nonresponsive to chest tube placement and antibiotic therapy. (*A*) Right lateral thoracic radiograph reveals thickening of the pleural surface with small regions of plural fluid accumulation and a small volume of free pleural gas. There is a chest tube placed in the caudal thorax. A region of alveolar opacity is identified within the caudal mediastinum just behind the cardiac silhouette. Within the caudodorsal lung fields is a well-circumscribed alveolar opacity with overlying gas opacity suggestive of a pulmonary abscess. This alveolar density was difficult to identify on the orthogonal projections. (*B*) CT image of the caudal thorax of the same cat. Two well-circumscribed alveolar densities with central gas opacities are identified at the periphery of the left and right caudal lung lobes (*). There is thickening of the adjacent pleural surfaces and pneumothorax. Surgery revealed compartmentalized caudal mediastinal and pleural fluid with pleuritis and focal abscessation of the right and left caudal lung lobes. Histopathologic examination revealed chronic, necrotizing and suppurative bronchopneumonia with foreign material and fibrosis and chronic necrosuppurative pleuritis with granulation tissue.

In patients with pyothorax undergoing contrast CT, pleural surfaces are often moderately to markedly contrast enhancing because of the marked thickening, hyperemia, and increased vascular permeability of the pleura. Pleural abscesses often appear as ring-enhancing cystic masses with a fluid-attenuating core, although central attenuation may be significantly higher (30–60 Hounsfield units) because of the cellular and protein content of abscess fluid. Mediastinal and tracheobronchial lymph nodes may also be easier to identify and differentiate from surrounding tissues on contrast-enhanced CT studies. Nodes tend to be moderately to markedly contrast enhancing and should generally have a uniform pattern of contrast enhancement. A central contrast void may be recognized that corresponds to fat within the lymph node hilus.

### *Pneumothorax*

Pneumothorax can result from trauma, foreign body migration, rupture of a pulmonary bulla or subpleural bleb, iatrogenic causes, visceral pleural erosion from underlying inflammatory lung disease, or necrosing neoplasia. Although pneumothorax is readily diagnosed using conventional radiography, the inciting abnormality is not easily recognized in patients, with the exception of traumatic and iatrogenic pneumothorax. Because the underlying cause of pneumothorax has an impact on treatment and prognosis, CT is often indicated in this subset of patients.

Spontaneous pneumothorax can be caused by rupture of a pulmonary bulla or subpleural bleb [19]. A bulla is defined as a region of vesicular emphysema located within the pulmonary parenchyma. A bleb is a thin-walled gas-filled structure that is located subpleurally and often arises as a sequela of air dissection from damaged alveoli [1,20]. Radiographically, bullae are characterized by a region of hyperlucency within the pulmonary parenchyma that may or may not include a thin rim of surrounding tissue. Blebs are similar in appearance to bullae; however, they are typically located at the apices of the lung and are subpleural [1]. Radiographic detection of blebs and bullae in dogs ranges from 0% to 50% [20]. This is likely attributable to superimposition of overlying anatomy surrounding a small gas-filled structure.

The CT findings associated with bullae and blebs in the dog include regions of low pulmonary parenchymal attenuation, disruption of the vascular pattern by pruning, and vascular distortion around areas of decreased attenuation (Fig. 9) [21]. Ruptured bullae and blebs often result in massive pneumothorax that may be unilateral or bilateral. Marked lung lobe atelectasis decreases lung volume, significantly increases pulmonary density, and obscures the underlying lesion. Patients undergoing CT for pneumothorax should have a chest tube placed before anesthesia to reduce the volume of pneumothorax and to reinflate an atelectatic lung. The pleural space should be evacuated and the study performed under mild positive-pressure ventilation to minimize atelectasis when possible. Although CT has been reported to be highly beneficial for the diagnosis of ruptured pulmonary bullae in patients with pneumothorax [21], in the authors' experience, CT has not been particularly rewarding in

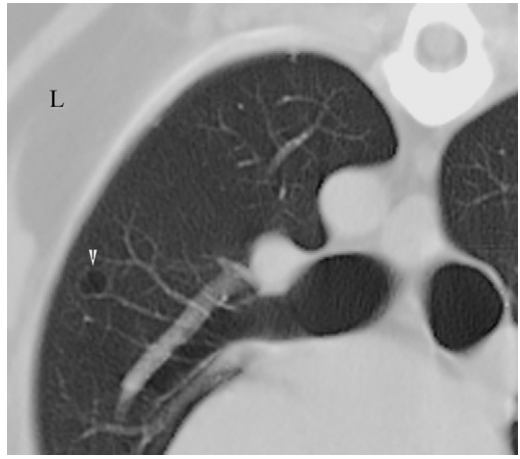


**Fig. 9.** CT image from an adult mixed-breed dog presented for a pulmonary mass. An incidental finding was a pulmonary bulla in the caudal subsegment of the left cranial lung lobe. Note the region of disrupted vasculature with a central region of hypoattenuation typical of pulmonary bullae (*arrowhead*).

localizing a ruptured bulla caused by persistent lobar atelectasis despite attempts to reinflate the lungs.

## Airway-Oriented Disorders

### *Bronchial foreign bodies*

Radiographic findings with bronchial foreign bodies are variable. If the foreign body is radiopaque, the diagnosis is often uncomplicated; however, diagnosis of radiolucent foreign bodies (eg, grass awns, sticks, wood) is not as simple. In the early stages of disease, radiographs of patients with nonradiopaque foreign bodies can appear normal. Radiographs become abnormal only after bronchial secretions accumulate or focal pneumonia develops. Common radiographic findings include focal interstitial pulmonary infiltrates with an accentuated bronchial pattern along a major bronchus, lobar or multifocal alveolar consolidations, focal bronchiectasis, pleural effusion with focal or multifocal pulmonary infiltrates, and pneumothorax (Fig. 10) [1].

The CT findings of bronchial foreign bodies are similar to the radiographic findings and include focal to multifocal (depending on the number of foreign bodies) interstitial to alveolar consolidations along an airway, focal lobar consolidation, focal bronchiectasis, pleural and mediastinal fluid accumulation, mild hilar and mediastinal lymphadenopathy, and pneumothorax. Given the superior contrast resolution of CT and its lack of superimposition of adjacent structures, nonradiopaque bronchial foreign bodies can occasionally be visualized.

### *Bronchial disease*

Acute bronchial or tracheobronchial disease in the dog is usually radiographically subtle or silent. Architectural and cellular abnormalities must occur to result in clinically significant radiographic changes. These abnormalities include edema and cellular infiltration of the bronchial mucosa and submucosa, mucus covering the bronchial walls, proliferation and hyperplasia of bronchial linings, and inflammation of the peribronchial tissues [1]. The principal radiographic sign of canine chronic bronchitis has been described as bronchial wall thickening. This is seen radiographically as an increased number of thickened bronchi, visible end-on as "donuts" and as parallel lines in the long axis. Depending on the severity and chronicity of disease, additional radiographic signs may include bronchiectasis and interstitial infiltrates with obscuring of the pulmonary vasculature [1]. These radiographic signs are a sequela of bronchial mucosal edema, hyperplasia, mucus accumulation, and inflammation of the peribronchial tissues [22]. As normal dogs age, histopathologic changes are evident radiographically as a diffuse interstitial pattern, pleural thickening, and bronchial wall mineralization [23]. Some texts consider these radiographic findings similar to those in dogs with chronic bronchitis, and because many dogs with chronic bronchitis are older, some authors consider radiographs to be a nonspecific test for chronic bronchitis [1]. A recent study [24] found that the sensitivity of radiographs for the diagnosis of canine chronic bronchitis ranged from 52% to 65%, the specificity was 91%, and the accuracy ranged

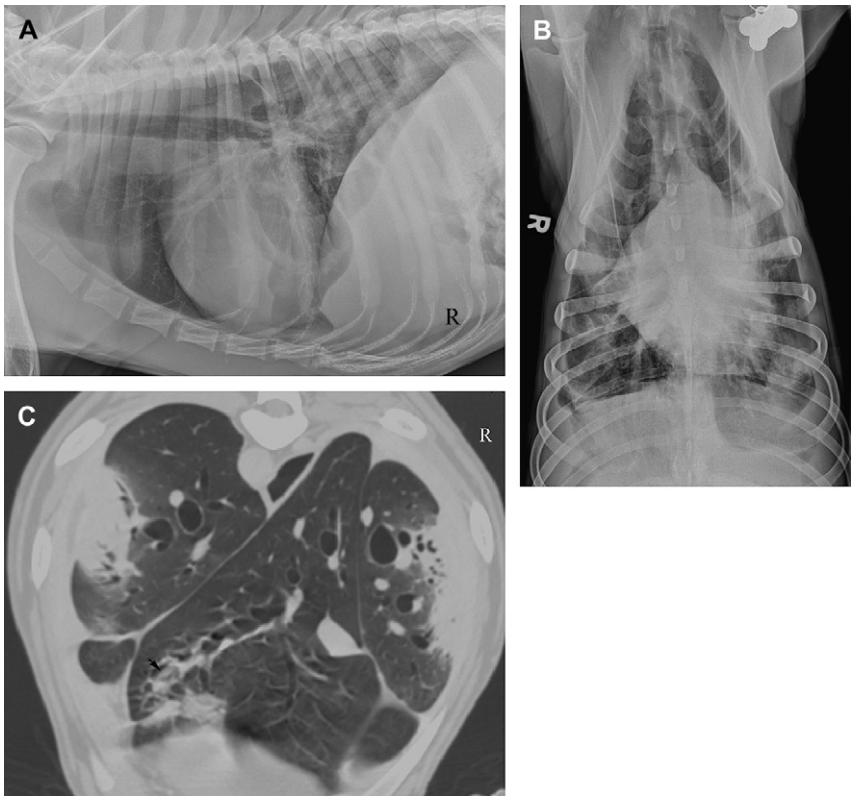


**Fig. 10.** Right lateral (*A*) and dorsoventral (*B*) radiographs from a 3-year-old German Short-Haired Pointer with a history of chronic cough. Interstitial to alveolar pulmonary infiltrates are identified within the left and right caudal lung lobes, right middle lung lobe, accessory lung lobe, and caudal subsegment of the left cranial lung lobe. Additionally, there are multiple focal regions of compartmentalized pleural effusion and thickening of the pleural surfaces. (*C*) Helical CT examination reveals multifocal regions of alveolar infiltrates within the right and left caudal lung lobes as well as in the accessory lung lobe. Multiple focal regions of bronchiectasis are also identified. A foreign body can be seen in the distal aspect of the accessory lung lobe (*arrow*). Bronchoscopy revealed multiple regions of bronchopneumonia with multiple grass awns within the airways and associated bronchiectasis.

from 65% to 74%. The most significant radiographic findings in that study supportive of chronic bronchitis were thickening of the bronchial walls and an increase in the number of bronchial wall shadows [24].

Thoracic CT may be much more accurate as an aid in the diagnosis of canine chronic bronchitis. By removing superimposing structures, individual bronchi can be more easily seen and more accurately characterized. Additionally, bronchial wall thickness can be directly measured on a computer workstation. Moreover, the peribronchial and interstitial tissues can be more accurately assessed for pathologic change.

Bronchiectasis is an airway-oriented condition characterized by persistent airway dilatation, often with suppuration. It is reported as a sequela to chronic uncontrolled infectious or inflammatory disease in dogs and cats. Radiographically, the disease can be recognized by thickened airway walls and dilated airways that fail to taper appropriately in the periphery. Focal pneumonia may also be present. In human and veterinary medicine, thoracic radiographs are insensitive for the diagnosis until late in the course of disease when irreversible changes have occurred. CT is the preferred method for diagnosis in human medicine, and the CT diagnosis of bronchiectasis is made using bronchial to adjacent pulmonary arterial diameter ratios. In the authors' experience in dogs with airway disease, a bronchial/arterial ratio of 2 or more is highly suggestive of bronchiectasis. Regions of increased interstitial pulmonary density can also be seen adjacent to the dilated bronchi (Fig. 11).

*Feline airway disease*

As with dogs, for pulmonary changes in cats to be evident radiographically, substantial cellular and architectural pulmonary changes must occur. In cats with chronic airway disease, these changes may include hyperplasia of the bronchial glands, bronchial wall cellular infiltration, hypertrophy of the bronchial smooth muscles, and, occasionally, bronchiectasis. Radiographic features of feline airway disease are similar to those in dogs and include increased

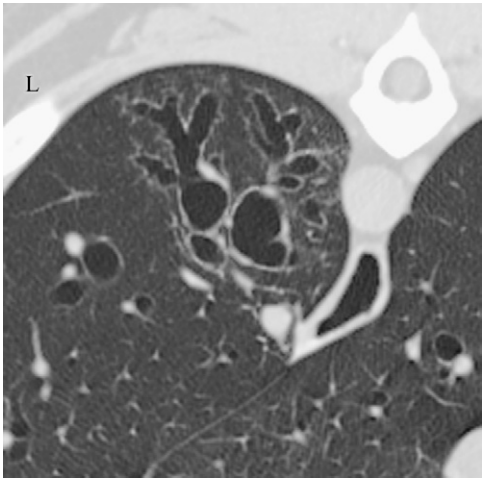


**Fig. 11.** CT image from an 8-year-old Labrador Retriever with a history of chronic cough and recurrent left caudal lung lobe infiltrates reveals focal bronchiectasis in the left caudal lung lobe with an irregular contour to the bronchial walls consistent with traction bronchiectasis. A ground-glass–like increase in interstitial pulmonary density is also identified adjacent to the dilated bronchi. Histopathologic examination of the affected lung revealed bronchiectasis, septal fibrosis, type II pneumocyte hyperplasia, alveolar histiocytosis, and lymphoplasmacytic peribronchitis. An underlying cause for the lesion was not determined, but it was most consistent with a previous pneumonia.

radiodensity and thickening of bronchial walls, increased visibility and numbers of bronchial markings, increased peribronchial radiodensity, a diffuse increase in interstitial pulmonary radiodensity, soft tissue accumulation in airways suggestive of mucus plugging, hyperinflation, collapse of the right middle lung lobe, and occasional bronchiectasis (Fig. 12) [1].

The CT findings in feline airway disease are similar to the radiographic features; however, given the lack of superimposition, this modality is likely more sensitive than conventional radiography. Soft tissue material deposited in airways (suggestive of mucus plugging) is more obvious with CT. Interstitial markings may appear multifocal and coalescing, and these opacities can resemble the ground-glass appearance that has been reported to represent active alveolitis or fibrosis in people (Fig. 13) [25]. Linear, parenchymal, soft tissue opacities that are nontapering and peripheral (similar to parenchymal bands identified in human beings) are also occasionally seen. These are thought to represent areas of atelectasis or fibrosis (Fig. 14) [26].

## Pulmonary Parenchymal Disorders

### *Pulmonary masses*

Conventional radiography is often used to identify thoracic masses but may be less useful for differentiating pulmonary, mediastinal, or thoracic wall origin and for localizing a pulmonary mass to a specific lung lobe. In addition, CT provides more accurate assessment of the likelihood of an inflammatory versus a neoplastic mass and for detecting mediastinal and hilar lymph node involvement [27]. Additional information provided by CT compared with traditional radiography includes defining mediastinal or pulmonary location of masses, the extent of lung pathologic change with delineation of lung versus pleural masses,

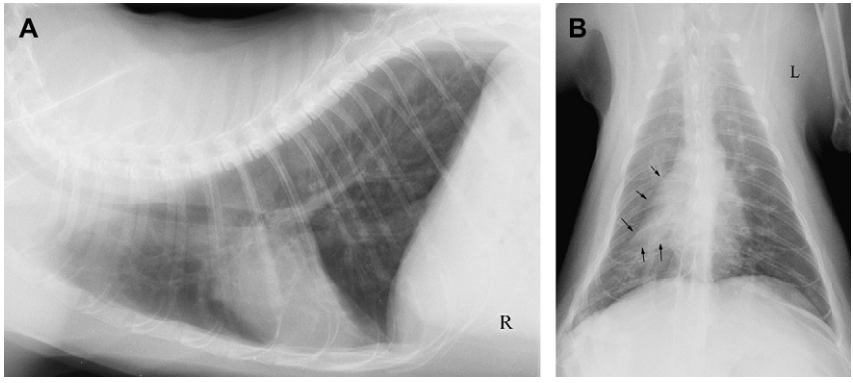


**Fig. 12.** Lateral (*A*) and dorsoventral (*B*) radiographs of a 3-year-old domestic short-haired cat with a history of coughing. There is a diffuse bronchial pattern with airway thickening identified in all lung fields. The patient is hyperinflated, and there is right middle lung lobe collapse (*arrows in B*). There is a diffuse increase in interstitial pulmonary radiodensity. The diagnosis was chronic airway disease.

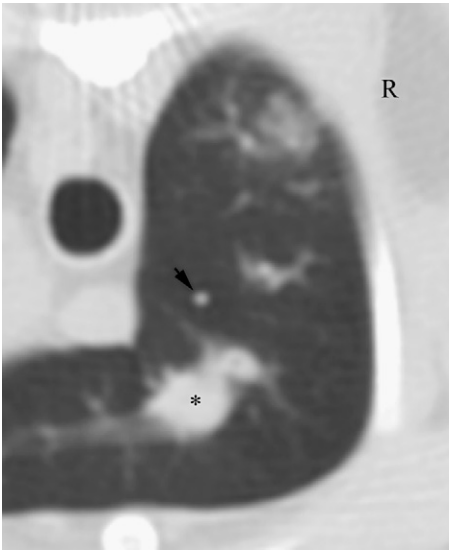


**Fig. 13.** CT image of a 5-year-old cat with a history of chronic coughing shows a large soft tissue density in the right cranial lung lobe bronchus consistent with an intraluminal mucus plug (*). A smaller mucus plug is seen immediately dorsally (*arrow*). Additionally, there are ground-glass pulmonary opacities present in the dorsal aspect of the right cranial lung suggestive of active alveolitis or fibrosis. These findings are consistent with chronic active airway disease.

the location of cavitated lung nodules, and the detection of bony lesions or pulmonary metastasis (Fig. 15) [15].

CT has been shown to be far more sensitive than conventional radiography for detecting pulmonary metastatic neoplasia in people [28]. Similarly, in dogs, only 9% of nodules detected with CT were identifiable on comparable thoracic radiographs [29]. CT allows detection of nodules that measure 1 mm in diameter versus conventional radiographs in which nodules must reach 7 to 9 mm before they are consistently detected (Fig. 16).

*Alveolar pulmonary disease*

An alveolar pulmonary pattern is caused by displacement of air from the pulmonary parenchyma. The radiographic characteristics of an alveolar pattern include air bronchogram formation; soft tissue opacification of lung; lobar consolidation; and silhouetting of adjacent soft tissue structures, including the heart and pulmonary vessels. The common disease processes associated with this pattern are bronchopneumonia, neoplasia, severe edema, and pulmonary hemorrhage.

CT can prove valuable in patients with chronic alveolar pulmonary consolidation that is nonresponsive to conventional therapies. It may reveal pulmonary masses obscured by overlying alveolar disease or small pulmonary nodules not visualized with conventional radiography [27,29]. Additionally,

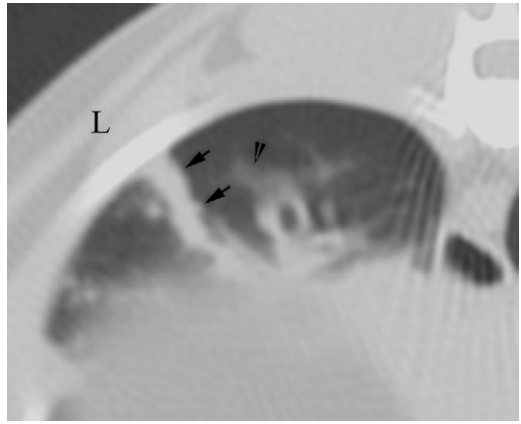


**Fig. 14.** CT image of the thorax of a young adult cat with a history of chronic coughing. There is a linear, nontapering, parenchymal soft tissue opacity in the left caudal lung lobe suggestive of fibrosis and scarring from associated chronic airway disease (*arrows*). Additionally, bronchial wall thickening and ground-glass opacities (*arrowhead*) are present, suggesting active alveolitis or fibrosis.

bronchial foreign bodies or pulmonary architectural abnormalities, such as bronchiectasis, that predispose patients to chronic recurrent pneumonia may be recognized. The peribronchial lymph nodes also can be more accurately assessed because they are better visualized with CT than with conventional radiography.

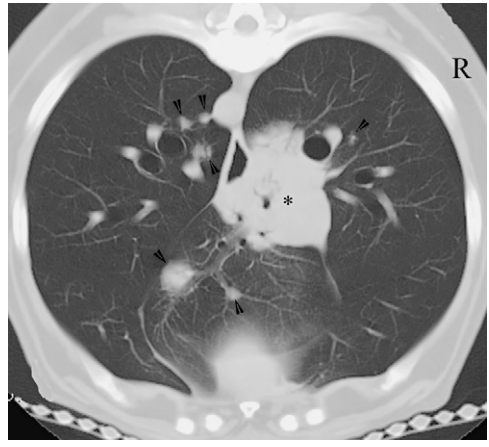


**Fig. 15.** CT image from an 11-year-old mixed-breed dog with a solitary pulmonary mass evident radiographically demonstrates a well-circumscribed pulmonary mass at the junction of the right caudal lung lobe bronchus and the accessory lung lobe bronchus (*). Additionally, several well-circumscribed pulmonary nodules are visible in multiple lung fields (*arrowheads*). Histopathologic examination revealed pulmonary adenocarcinoma with intrapulmonary metastases.


**Fig. 16.** Helical CT image of a 12-year-old Collie with a bleeding splenic mass demonstrates multiple soft tissue nodules within the pulmonary parenchyma (*arrows*). Atelectasis is noted in the caudal subsegment of the left cranial lung lobe (*), illustrating the need for a forced breath hold to avoid obscuring pulmonary pathologic findings. Histopathologic examination revealed splenic hemangiosarcoma with pulmonary metastases to the lungs.

### *Diffuse pulmonary disease*

The CT characteristics of diffuse pulmonary disease are not well described in the veterinary literature. Caution should be exercised in drawing too many parallels with CT patterns described in human beings because of the anatomic differences in the subgross lung anatomy of dogs and cats.

### *Canine idiopathic pulmonary fibrosis*

Interstitial lung disease is a poorly understood and characterized disease in the dog and cat [30]. Canine idiopathic pulmonary fibrosis (CIPF) is most apparent in middle-aged to geriatric dogs and seems to be overrepresented in West Highland White Terriers [31]. Alveolar septal thickening seems to be the predominant change identified histopathologically [30,31]. Radiographic findings include a diffuse interstitial pattern that sometimes may be miliary. Lung fields often appear to be hypoinflated secondary to decreased pulmonary compliance. Occasionally, right heart enlargement and associated pulmonary arterial enlargement can be identified as a sequela to secondary pulmonary hypertension (Fig. 17).

Recently high-resolution CT has been used to evaluate suspected cases of CIPF [32]. Unfortunately, only small numbers of dogs have CT images and concurrent histopathologic confirmation of CIPF. CT findings considered consistent with CIPF include ground-glass opacity, traction bronchiectasis, interstitial thickening, and honeycombing [32]. Ground-glass opacity is defined as an increase in lung opacity that does not obscure underlying vessels. This finding may indicate active alveolar inflammation or fibrosis [33]. Traction bronchiectasis is characterized by bronchial dilation with an irregular contour.

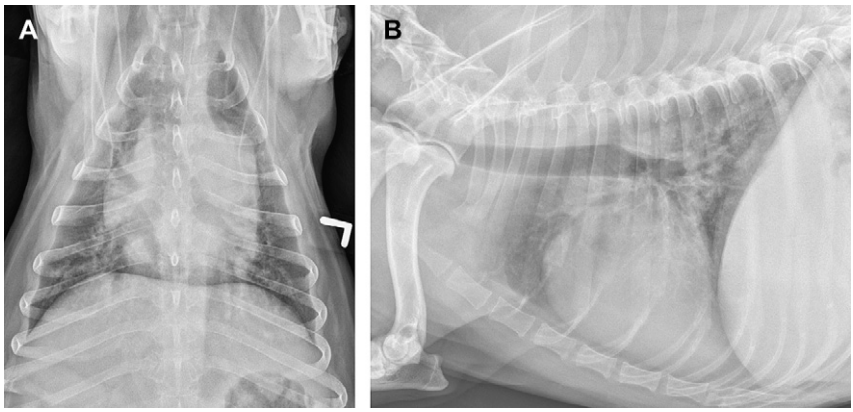


**Fig. 17.** Right lateral (*A*) and dorsoventral (*B*) radiographs of a 13-year-old terrier cross presented with a history of tachypnea. There is a diffuse heavy interstitial pattern with a mild underlying bronchial pattern. These radiographs were taken at maximum inspiration, and the patient is hypoinflated, suggesting decreased pulmonary compliance. There is moderate right heart enlargement with mildly enlarged pulmonary arteries. Necropsy with histopathologic examination revealed extensive multifocal primary interstitial pulmonary fibrosis with right heart hypertrophy suggesting secondary pulmonary hypertension.

It is thought to result from traction on the bronchial wall secondary to fibrosis of the lung parenchyma [34]. Honeycombing is defined by cystic air-filled spaces several millimeters in diameter that are often peripheral, and in human medicine, this indicates dissolution of alveoli and loss of architecture [32].

### *Coccidioidomycosis*

Coccidioidomycosis is caused by *Coccidioides immitis,* a dimorphic fungus endemic to the southwestern United States. The most frequent primary site of infection is the lung. The radiographic features of coccidioidomycosis are similar to those of other fungal diseases and include peribronchial, micronodular pulmonary lesions (miliary pulmonary pattern), ill-defined pulmonary consolidations, or occasional lobar consolidations. Tracheobronchial and mediastinal lymphadenopathy is a common feature [1].

The CT features of pulmonary coccidioidomycosis are similar to the radiographic features. Tracheobronchial and mediastinal lymphadenopathy are easier to identify with CT because of the removal of superimposed structures (Fig. 18).

## SUMMARY

Although conventional radiography is still the first diagnostic imaging approach to respiratory disease, CT is proving to be invaluable as an adjunctive procedure in characterizing nasal and thoracic pathologic findings. CT eliminates superimposition of overlying structures and offers superior contrast resolution as compared with conventional radiography. These advantages

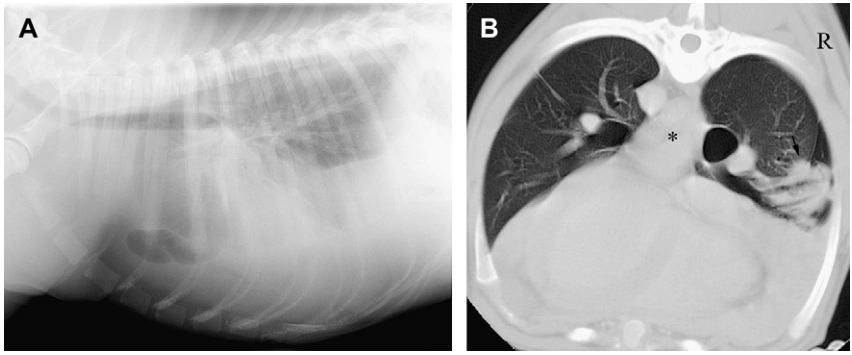


**Fig. 18.** (*A*) Right lateral radiograph of a 1-year-old Labrador Retriever with a history of decreased appetite and mild respiratory distress reveals marked pleural effusion with rounding of the lung margins suggestive of chronic inflammatory pleural effusion. Alveolar infiltrates in the left cranial lung lobe may represent atelectasis or bronchopneumonia. (*B*) CT examination of the same patient reveals loculated pleural and mediastinal fluid accumulation with ill-defined alveolar pulmonary infiltrates in the right middle lung lobe (*arrow*). Hilar lymphadenopathy is present between the mainstem bronchi (*). Histopathologic examination revealed marked chronic pyogranulomatous mediastinitis and chronic pyogranulomatous pneumonia within the right middle lung lobe. Both regions contained intralesional fungal spherules of *Coccidioides immitis*.

allow for more precise characterization and localization of lesions and are invaluable for guiding rhinoscopic, bronchoscopic, and surgical procedures.

## References

[1] Suter PF. Thoracic radiography a text atlas of thoracic diseases of the dog and cat. Wettswil (Switzerland): P.F. Suter; 1984.
[2] Saunders JH, Van Bree H, Gielen I, et al. Diagnostic value of computed tomography in dogs with chronic nasal disease. Vet Radiol Ultrasound 2003;44(4):409–13.
[3] Sullivan M, Lee R, Jakovljevic S, et al. The radiological features of aspergillosis of the nasal cavity and frontal sinuses in the dog. J Small Anim Pract 1986;27:167–80.
[4] Saunders JH, Zonderland JL, Clercx C, et al. Computed tomographic findings in 35 dogs with nasal aspergillosis. Vet Radiol Ultrasound 2002;43(1):5–9.
[5] Saunders JH, Van Bree H. Comparison of radiography and computed tomography for the diagnosis of canine nasal aspergillosis. Vet Radiol Ultrasound 2003;44(4):414–9.
[6] Wilkinson GT. Feline cryptococcosis: a review and seven case reports. J Small Anim Pract 1979;20:749.
[7] Tomsa K, Glaus TM, Zimmer C, et al. Fungal rhinitis and sinusitis in three cats. J Am Vet Med Assoc 2003;222(10):1380–4.
[8] Harvey CE, Biery DN, Morello J, et al. Chronic nasal disease in the dog: its radiographic diagnosis. Veterinary Radiology 1979;20:91–8.
[9] Schwartz T. Comparison of sensitivity and specificity of conventional radiography and computed tomography (CT) in nasal tumors and fungal rhinitis in dogs. Vet Radiol Ultrasound 1995;36:428.
[10] Burk RL. Computed tomographic imaging of nasal disease in 100 dogs. Vet Radiol Ultrasound 1992;33(3):177–80.
[11] Madewell BR, Priester WA, Gillette EL, et al. Neoplasms of the nasal passages and paranasal sinuses in domesticated animals as reported by 13 veterinary colleges. Am J Vet Res 1976;37:851–6.

[12] Schoenborn WC, Wisner ER, Kass PH, et al. Retrospective assessment of computed tomographic imaging of feline sinonasal disease in 62 cats. Vet Radiol Ultrasound 2003;44(2):185–95.
[13] O'Brien RT, Evans SM, Wortman JA, et al. Radiographic findings in cats with intranasal neoplasia or chronic rhinitis: 29 cases (1982–1988). J Am Vet Med Assoc 1996;208(3):385–9.
[14] Rebner M, Gross BH, Robertson JM, et al. CT evaluation of mediastinal masses. Comput Radiol 1987;11:103–10.
[15] Prather AB, Berry CR, Thrall DE. Use of radiography in combination with computed tomography for the assessment of noncardiac thoracic disease in the dog and cat. Vet Radiol Ultrasound 2005;46(2):114–21.
[16] Bilbrey SA, Birchard SJ. Pulmonary lymphatics in dogs with experimentally induced chylothorax. J Am Anim Hosp Assoc 1994;30:86–91.
[17] Esterline ML, Radlinsky MG, Biller DS, et al. Comparison of radiographic and computed tomography lymphangiography for identification of the canine thoracic duct. Vet Radiol Ultrasound 2005;46(5):391–5.
[18] Johnson EG, Wisner ER, Marks SL, et al. Contrast enhanced CT thoracic duct lymphography. Paper presented at: the annual conference of the American college of veterinary radiology. Chicago: 2006.
[19] Lipscomb VJ, Hardie RJ, Dubielzig RR. Spontaneous pneumothorax caused by pulmonary blebs and bullae in 12 dogs. J Am Anim Hosp Assoc 2003;39:435–45.
[20] Puerto DA, Brockman DJ, Lindquist C, et al. Surgical and nonsurgical management of and selected risk factors for spontaneous pneumothorax in dogs: 64 cases (1986–1999). J Am Vet Med Assoc 2002;220:1670–4.
[21] Au JJ, Weisman DL, Stefanacci JD, et al. Use of computed tomography for evaluation of lung lesions associated with spontaneous pneumothorax in dogs: 12 cases (1999–2002). J Am Vet Med Assoc 2006;228(5):733–7.
[22] Wheeldon EB, Pirie HM, Fisher EW. Chronic bronchitis in the dog. Vet Rec 1974;94:466–71.
[23] Reif JS, Rhodes WH. The lungs of dogs: a radiographic-morphologic correlation. Journal of the American Veterinary Radiologic Society 1966;7:5–11.
[24] Mantis P, Lamb CR, Boswood A. Assessment of the accuracy of thoracic radiography in the diagnosis of canine chronic bronchitis. J Small Anim Pract 1998;39:518–20.
[25] Muller NL, Stales CA, Miller RR, et al. Fibrosing alveolitis: CT-pathologic correlation. Radiology 1986;160:585–8.
[26] Webb WR. High-resolution lung computed tomography. Normal anatomic and pathologic findings. Radiol Clin North Am 1991;29:1058–63.
[27] Spann DR, Sellon RK, Thrall DE, et al. Computed tomographic diagnosis: use of computed tomography to distinguish a pulmonary mass from alveolar disease. Vet Radiol Ultrasound 1998;39(6):532–5.
[28] Berman CG, Clark RA. Diagnostic imaging in cancer. Prim Care 1992;19(4):677–713.
[29] Nemanic S, London CA, Wisner ER. Comparison of thoracic radiographs and single breath-hold helical CT for detection of pulmonary nodule in dogs with metastatic neoplasia. J Vet Intern Med 2006;20(3):508–15.
[30] Lobetti RG, Milner RR, Muller NL. Chronic idiopathic pulmonary fibrosis in five dogs. J Am Anim Hosp Assoc 2001;37:119–27.
[31] Corcoran BM, Dukes-McEwan J, Rhind S, et al. Idiopathic pulmonary fibrosis in a Staffordshire bull terrier with hypothyroidism. J Small Anim Pract 1999;40:185–8.
[32] Johnson V, Corcoran BM, Wotton PR, et al. Thoracic high-resolution computed tomographic findings in dogs with canine idiopathic pulmonary fibrosis. J Small Anim Pract 2005;46:381–8.
[33] Leung AN, Miller RR, Muller NL. Parenchymal opacification in chronic infiltrative lung diseases: CT-pathologic correlation. Radiology 1993;188:209–14.
[34] Westcott JL, Cole SR. Traction bronchiectasis in end-stage pulmonary fibrosis. Radiology 1986;161(3):665–9.